Large-Scale Robust Quantum Dot Microdisk Lasers with Controlled High Quality Cavity Modes

*Chun Hao Lin, Qingji Zeng, Evan Lafalce, Marcus J. Smith, Sidney T. Malak, Jaehan Jung, Young Jun Yoon, Zhiqun Lin, Zeev Valy Vardeny, and Vladimir V. Tsukruk**

This study reports a facile on-chip fabrication of CdSe/$Cd_{1-x}Zn_xSe_{1-y}S_y$ quantum dot microdisk lasers and their large-area arrays via a pattern-assisted layer-by-layer assembly process. This approach combines the versatility of colloidal semiconducting nanoparticles (bright emission, solubility, and high stability) with the spatial precision of optical lithography to create robust large-area optical lasing arrays (up to a few thousand disks). Specifically, microdisk lasers with high quality factors (within 1000–2000) are fabricated with predefined size and shape (as controlled by master templates) with high consistency and throughput, essentially providing a new approach to fabricate difficult-to-control on-chip optical cavities in a low-cost and effective manner. Notably, the number of longitudinal cavity modes in the microdisk laser can be precisely controlled by varying the microdisks' diameter, allowing for either near-single mode or multimode operation while preserving high quality factors. Furthermore, the cross-linking of quantum dots imparts high chemical resistance and mechanical robustness that helps retain the structural integrity under harsh processing conditions (such as sonication or direct exposure to various solvents). As such, these quantum dot microdisk laser arrays are promising candidates for advancing the development of large-area, low-cost on-chip photonic structures with controlled lasing modes.

1. Introduction

Direct band gap semiconductor lasers have received much attention due to their inherently efficient optical gain performance and stability.[1] The promising lasing properties have enabled the development of essential commercial technologies including fiber-optic communication, high power laser operation at varying wavelengths, and barcode scanners.[1] Current research has focused on the miniaturization of semiconductor lasers that can lead to smaller, cheaper, and more sensitive high performance on-chip photonic cavities, including a variety of micro- and nanoscale lasers of different geometries.[2–4] These miniaturized photonic cavities can be tailored to manipulate the resonant optical modes within the cavity via total internal reflection or light oscillation between reflective end facets.[5] More importantly, microdisks may enable the development of novel photonic microcavities that judiciously utilize the evanescent field extending hundreds of nanometers from the cavity boundary to control light transport. This type of control has potential applications in parity-time (PT) symmetry microcavities,[6] and can significantly enhance the detection sensitivity of sensing elements based upon whispering gallery modes in photonic cavities down to single particle limits.[7] Furthermore, these unique properties may further support the development of future information processors and ultrasensitive sensors due to the nonreciprocal light transmission and high refractive index contrast with the surrounding medium.[29]

Compact semiconductor photonic cavities are often fabricated using either top-down[8] or bottom-up[9] approaches. The top-down approach typically involves a lithographic process (e.g., photolithography or electron beam lithography (EBL)[42]) to predefine the surface of deposited active semiconductor layers. A patterned photoresist provides protection from an etching process (using appropriate selection of conditions), which subsequently removes the material that is not protected. Depending on the resolution of the photoresist, micro- and even nanoscale cavities with well-defined geometry can be reliably fabricated. The ability to control the spatial dimensions of the photonic structures is essential for realizing practical and robust on-chip photonic circuits, and is a primary reason these top-down approaches are utilized. However, these top-down lithography approaches often require complicated microfabrication processes under clean-room conditions and expensive facilities in order to properly etch or deposit the materials.[10]

On the other hand, the bottom-up approach offers facile and low-cost assembly of high quality colloidal photonic cavities directly on the desired substrate via the self-assembly and

Dr. C. H. Lin, Dr. M. J. Smith, Dr. S. T. Malak, Dr. J. Jung, Dr. Y. J. Yoon, Prof. Z. Lin, Prof. V. V. Tsukruk
School of Materials Science and Engineering
Georgia Institute of Technology
Atlanta, GA 30332, USA
E-mail: Vladimir@mse.gatech.edu
Dr. Q. Zeng, Dr. E. Lafalce, Prof. Z. V. Vardeny
Department of Physics and Astronomy
University of Utah
Salt Lake City, UT 84112, USA
Dr. M. J. Smith
Aerospace Systems Directorate
Air Force Research Laboratory
Wright-Patterson Air Force Base
OH 45433, USA

DOI: 10.1002/adom.201700011

crystallization process. Colloidal cavities assembled using the bottom-up approach have been shown to possess good lasing performance (quality factors ($\lambda/\delta\lambda$) on the order of 10^3) and low lasing thresholds (down to a few hundred nJ cm^{-2}).[11] The impressive lasing characteristics have made them promising candidates for flexible compact semiconductor lasers with low lasing thresholds (≈μJ cm^{-2}).[47] However, at the present time, precise control of the size, shape, and location of these bottom-up colloidal cavities is challenging since the local crystallization and assembly processes depend critically on local temperature gradients, concentration of precursors, and pressure.[12] These obstacles severely hinder the integration of these cavities into practical flexible on-chip photonic circuits that may require optical cavities with specific dimensions and location.

Common optical emitting nanomaterials for flexible lasing structures include organic dyes, semiconducting nanoparticles, conjugated polymers, and perovskite materials.[13,43,46] Among them, Cd-based colloidal quantum dots (QDs) with dimensions below 10 nm are known to exhibit bright, size-tunable emission due to the quantum confinement effect.[14–16] Importantly, they possess high optical gain while maintaining lasing stability under optical pumping.[17,18] Moreover, they are solution-processable and therefore can be used in cost effective approaches and in a variety of applications to develop low-cost optoelectronic devices. For these reasons, a variety of QD cavities have been fabricated to date, in most cases by filling QDs into or coating QDs onto microcapillary tubes[19,20] or onto the silica microspheres.[21,22] Although cavity modes were observed in these QD photonic structures, it is difficult to integrate these types of structures into on-chip photonic circuits, on flexible substrates, or over large-scale areas.

Among recent examples, an attempt was made to fabricate microdisks of QDs sandwiched between silicon nitride (SiN) layers using a top-down approach with the assistance of photolithography.[23] Although a notable development, this approach requires careful selection and optimization of etching gas mixtures as well as a relatively expensive chemical vapor deposition system to deposit SiN layers. In addition, the high processing temperature for the deposition of SiN can alter the spectral position and quantum yield of the QDs.[24] Overall, the current individual implementation of top-down and bottom-up approaches cannot address many of the critical obstacles associated with micro- and nanoscale semiconductor cavities.

Here we present an efficient hybrid top-down/bottom-up approach via a pattern-assisted layer-by-layer (LbL) assembly process to fabricate large-area on-chip quantum dot microdisk laser arrays.[25–27] Utilization of QD nanoparticles along with the pattern-assisted LbL assembly enables the facile and vacuum-free fabrication of robust photonic cavities with predefined size, geometry, and location over a large scale in a simple manner, which is not an easy task for conventional top-down approaches or current bottom-up approaches. Importantly, this patterning approach represents a significant improvement in throughput and can be upscalable, with fast fabrication of thousands structures per hour which is much higher than previous studies using focused ion beam milling and EBL due to the parallel nature of the process. Furthermore, fabricated structures exhibit exceptional uniformity (size variation below 5%) over cm^2 areas, demonstrating the ability to precisely control the dimensions of fabricated structures. In addition, the high chemical resistance and mechanical strength of the microstructures, imparted via chemical cross-linking of functionalized quantum dots, allow them to withstand severe conditions such as sonication and direct exposure to harsh solvents. Furthermore, intense lasing behavior with high quality factors of 1000–2000 was observed, with the number of cavity modes and their mode spacing readily controlled by varying the disk radius. The ability to control the dimension and spatial distribution of robust and large-area cavity arrays, while maintaining high quality factors, may provide a platform for the development of novel PT photonic systems that may exhibit exceptional points for single-mode lasing and directional light propagation.[28,29]

2. Results and Discussion

2.1. Fabrication of Disk Arrays

We adopted a facile one-pot method (with some modification) to synthesize red-emitting core/graded shell CdSe/$Cd_{1-x}Zn_xSe_{1-y}S_y$ QDs with an average diameter of 7.7 ± 0.7 nm. (Figure S1, Supporting Information) (see the Experimental Section for detailed synthesis procedure).[30] The graded shell of QDs has been shown to effectively suppress Auger recombination, which is a primary obstacle for achieving optical gain from QDs.[31,32] Moreover, to fabricate mechanically robust QD microstructures, we used a solid state exchange process that tethers neighboring QDs via bifunctional cross-linkers to create highly cross-linked network that imparts mechanical strength and chemical resistance.[33]

The pattern-assisted LbL assembly used here to fabricate the QD photonic cavities includes several steps. First, circular microholes with a depth of 300 nm were fabricated in a photoresist using a standard photolithography process (**Figure 1**, steps 1–4).[34] Then, these microholes were subsequently filled with functionalized QDs using a spin-assisted LbL assembly by repeating deposition steps in a controlled sequential manner.[26,35] This deposition process was repeated until the structure achieved the desired thickness within the range of 100–200 nm, as monitored after the completion of fabrication process. The disk thickness grows linearly with the number of deposition cycles, as expected for LbL assembly with an increment of 25–30 nm per layer (Figure S2, Supporting Information).[36]

Assembled layers of close-packed QDs within fabricated thin disks were tethered to each other via the solid state ligand exchange process suggested in our previous study (Figure 1, step 5).[33] During this process, the capping ligand butylamine (BA) was replaced with the bifunctional cross-linker 1,7 diaminoheptane (DIAH) and the neighboring QDs were cross-linked via the strong coordination between QDs and amino end groups of DIAH.[33] Importantly, the DIAH cross-linking process imparts robustness to the QD microdisks, which prevents cracking under sonication during the removal of the photoresist (lift-off process) (Figure 1, step 6) and facilitates the mechanical integrity of the structures (Figure S3, Supporting Information). It is also worth mentioning that the underlying CYTOP layer acts as potentially important prime layer for fabrication on a

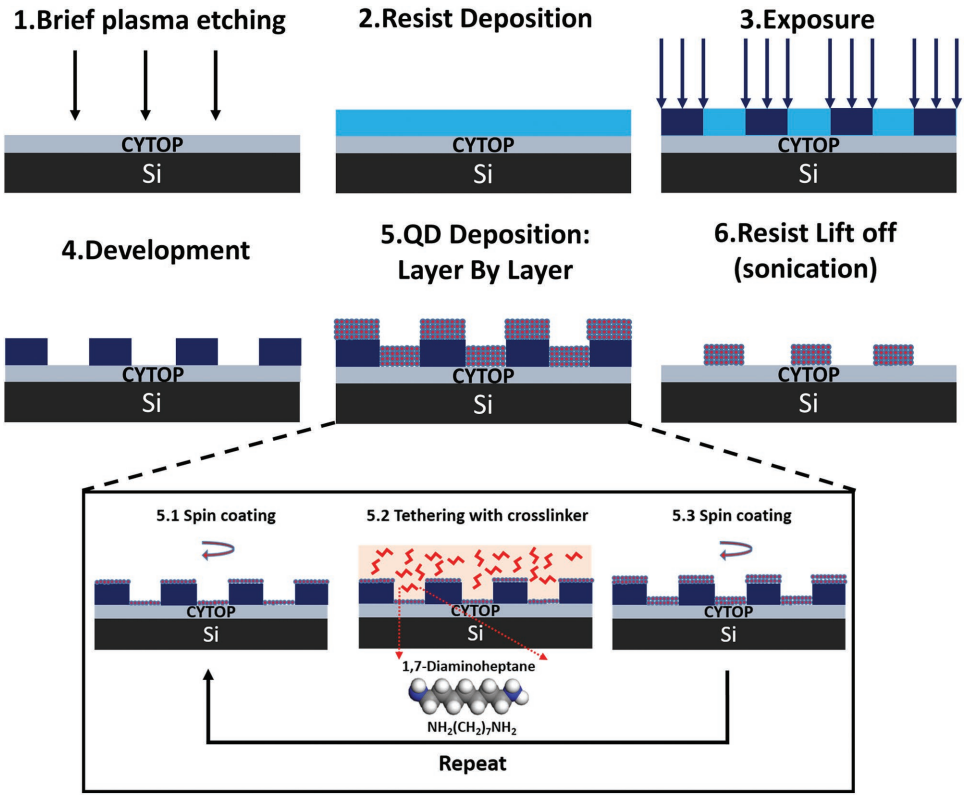

Figure 1. Schematic outlining the hybrid top-down/bottom-up approach using a pattern-assisted LbL assembly of QDs that used to fabricate the QD microdisks.

variety of substrates due to its low refractive index, mechanical robustness, and chemical resistance to different solvents (polar and nonpolar).

With this method, large-area organized arrays composed of a few thousand QD microstructures with predefined shape, size, and location can be fabricated in less than an hour (**Figure 2** and Figure S4 (Supporting Information)). Furthermore, because the microdisks are composed of a cross-linked QD network, they are chemically resistant to polar and nonpolar solvents.[33] This is a particularly desirable property if the microdisks are exposed to chemically harsh environments during the lift-off process or should operate under variable environment conditions. It is worth noting that the chemical stability of microdisks is in stark contrast to the conventionally fabricated colloidal cavities that are prone to dissolution in polar solvents (e.g., perovskite cavities).[37,38]

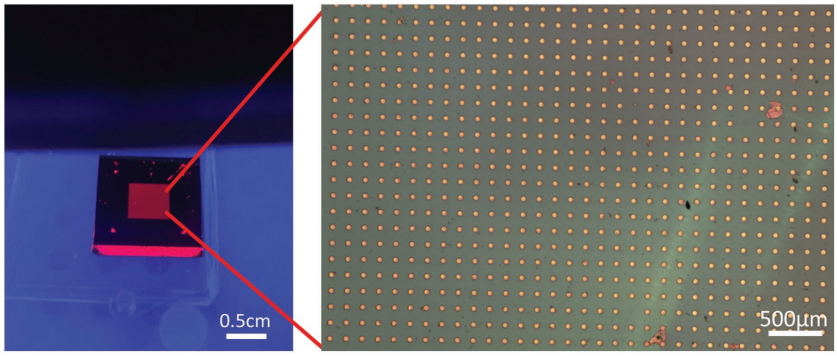

Figure 2. Left: optical micrograph of a substrate under UV illumination with an array of microdisks (diameter of 52.1 µm). Right: bright field image of a microdisk array at higher magnification.

2.2. Characterization of Disk Morphology

Figure 3a,b shows a series of fabricated QD microdisks with diameters ranging from 10 to 52 µm. In general, the size and location of the microdisk arrays closely match the original mask patterns (within 5%) (Figures 2 and 3 and Figure S4 (Supporting Information)). The shape of all fabricated microdisks, which is predefined by the patterned microholes in the photoresist, is almost perfectly circular with minimal density of defects and smooth side walls (Figure 2d).

The morphology of the fabricated microdisks was further investigated using atomic force microscopy (AFM). It was found that the microdisks actually possess a peculiar nest-like shape with elevated rims, a common feature of a flow- and evaporation-driven assembly of colloidal and polymeric materials, generally known as coffee-ring

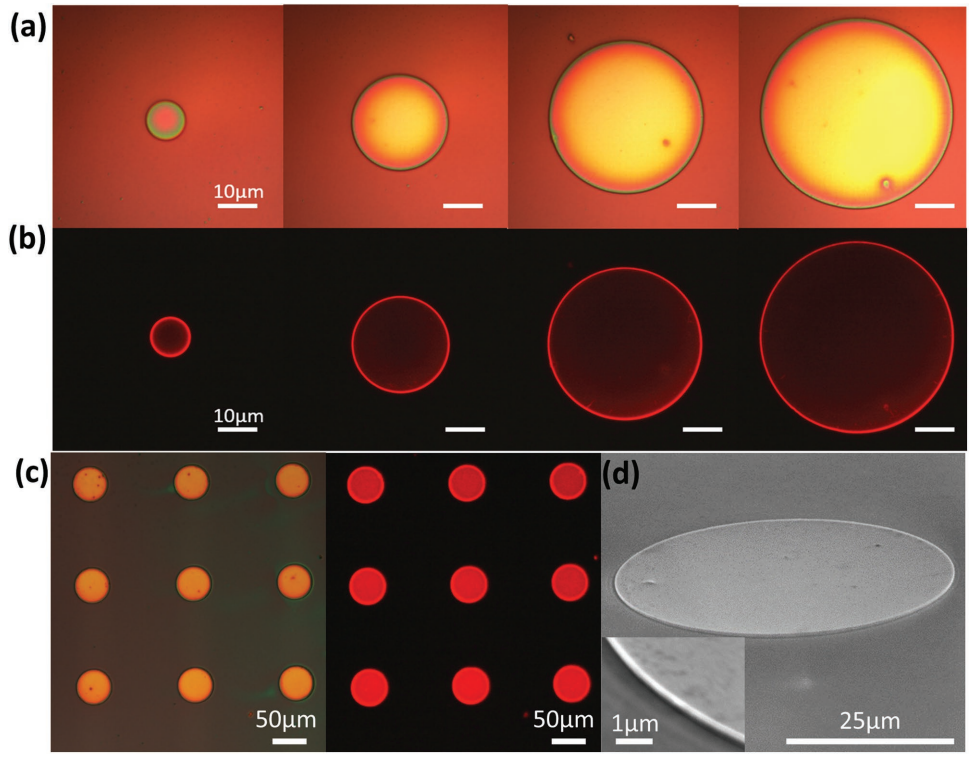

Figure 3. a) Bright field and b) PL imaging of QD microdisks with diameters of 10.6, 26.0, 41.6, and 52.1 μm. c) Bright field image (left panel) and PL image (right panel) of a 3 × 3 disk array (52.1 μm in diameter). d) SEM of a microdisk (inset: side wall).

effect, with fluidic flow under confined spaces (**Figure 4**).[39–41] This inhomogeneous distribution did not noticeably affect the global disk-like shape since the boundaries of the microholes were well-defined by the photolithography process and the rims compose only a small fraction of the microdisk volume. Generally, the rim height (270–280 nm) is close to the depth of microfabricated holes in the photoresist (≈300 nm), while the thickness of the uniform central region of the disk is about half of this value: around 100 nm for larger disks (>26 μm) and around 150 nm for the smallest disk (10.6 μm).

2.3. Optical Properties and Lasing Behavior

Optical characterization was performed by pumping the microdisks with a 532 nm, 7 ps pulsed laser in a confocal microphotoluminescence set-up (see the Experimental Section). We observed that an increase of pump fluence causes an increase of the optical gain from the QD microdisks, which eventually surpasses the optical loss and leads to consequently the onset of light amplification (amplified spontaneous emission (ASE) threshold) and intense lasing behavior when inside an optical cavity such as the microdisks. This nonlinear behavior leads to the appearance of sharp spectral peaks (due to optical cavity modes) over the broad spontaneous emission band once threshold is exceeded, confirming the occurrence of lasing action in the fabricated microdisks (**Figure 5**).

This nonlinear optical behavior can also be observed in the power–power plot where the microdisk studied (example is shown for 26.0 μm disk) shows an abrupt change from a linear pump dependence to a superlinear pump dependence (on the log–log scale) at the ASE threshold (**Figure 6**a).

In general, the ASE thresholds for microdisks of different diameter are found to be on the same order of magnitude (29–90 μJ cm^{-2}), which are comparable to the best values reported in literatures.[14,23] It is also worth noting that in ≈87% of the microdisks, the appearance of cavity mode splitting was observed at threshold (Figure S5, Supporting Information). Scattering centers that are responsible for the mode splitting can be clearly seen as bright spots in Figure 6b.

For one of the smaller microdisk, 10.6 μm, we observed mode-splitting at intensities significantly higher than the threshold value. We suggest that the smaller circumference limits the amplification of laser modes and causes the inability of the resonators to sustain high light intensities for lasing. The mode splitting could possibly be related to local heating and annealing near the circumference (namely the rim area) when the pump fluence is the highest. The specific mechanisms underlying this behavior are part of an ongoing study.

The cavity mode spacings ($\Delta\lambda$) of QD microdisks with different sizes decrease as the disk diameter increases while at the same time the number of resonant longitudinal cavity modes gradually increases in agreement with theory (see below) (**Figure 7**).[42] Moreover, near-single mode and multimode behavior can be readily controlled by varying the diameter of the fabricated QD microdisk in the relation with the gain spectrum of QDs and $\Delta\lambda$ (Figure 7). Importantly, the much narrower gain spectrum (≈30 nm) for QDs compared with those of organic dye molecules (≈30–100 nm)[43] can be advantageous to achieve the near-single mode operation over a wider range of

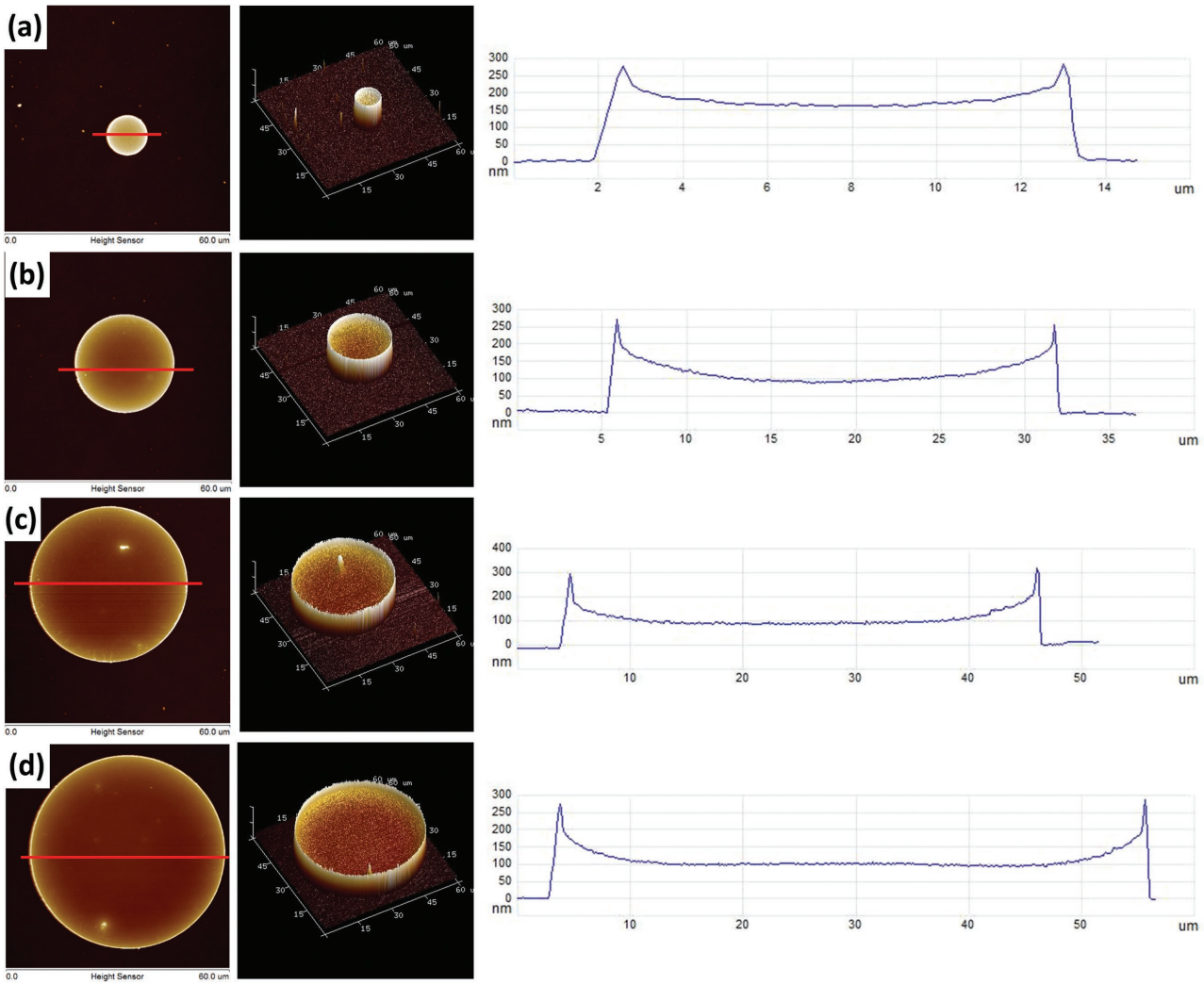

Figure 4. From left to right: AFM topographical images (top-view), 3D projection, and height cross-section profiles of QD microdisks with diameters of a) 10.6 µm, b) 26.0 µm, c) 41.6 µm, and d) 52.1 µm, respectively.

disk sizes, providing more flexibility on the structure design. In addition, the readily accessible near-single mode and multimode operation of this system could be extremely useful when trying to accommodate specific needs in a wide range of applications, including optical communication (single mode) and nanoparticle detection (multimode).[1,44]

The relationship between mode spacing ($\Delta\lambda$) and cavity length (L) can also provide detailed information on the cavity type and the effective refractive index of the microdisks.[42] The behavior of cavity modes can be estimated using the well-known equation, $\Delta\lambda = \lambda^2/2nL$, where λ is the peak wavelength of the cavity mode, n is the effective refractive index of QDs, and $2L$ is the optical path (round-trip) length.[45] The optical path length $2L$ in a microdisk cavity is represented by the circumference length, πD, which gives a modified equation of $\Delta\lambda = \lambda^2/n\pi D$.[45] Our study, indeed, confirms a linear relationship between mode spacing ($\Delta\lambda$) and the reciprocal optical path length $1/\pi D$ (**Figure 8**a). From this relationship, the effective refractive index of microdisks, n, at λ = 642 nm (dominant mode of ≈50% microdisks), can be estimated from the slope. The value obtained from this analysis, 1.88 ± 0.02, is in good agreement with the experimental value n = 1.90 measured from the uniform QD film by spectroscopic ellipsometry.[33] This refractive index value indicates that the propagating light is confined inside the cavity and that total internal reflection occurs in the region near the circumference of the QD microdisks; substantiating the claim that the fabricated microdisks are, indeed, whispering gallery mode resonators.

A more accurate effective refractive index of the microdisks (of different diameter) can be estimated using the Fourier transform of the emission spectrum, which contains equally spaced Fourier components with periodicity $\Delta l = n\pi D$ (**Figure 9**).[46] The path length (Δl) of microdisks from small to large diameters are determined to be 60.8 ± 1.3, 147.4 ± 1.3, 262.0 ± 0.1, 325.6 ± 0.1 µm, respectively. These values correspond to n of 1.82 ± 0.04 (10.6 µm), 1.81 ± 0.02 (26.0 µm), 2.00 ± 0.00 (41.6 µm), and 1.99 ± 0.00 (52.1 µm), showing that the larger disks (41.6, 52.1 µm) have higher effective refractive index (≈2) than that of the smaller disks (10.6 µm with n of ≈1.81 and 26.0 µm with n of ≈1.82, respectively). The difference in

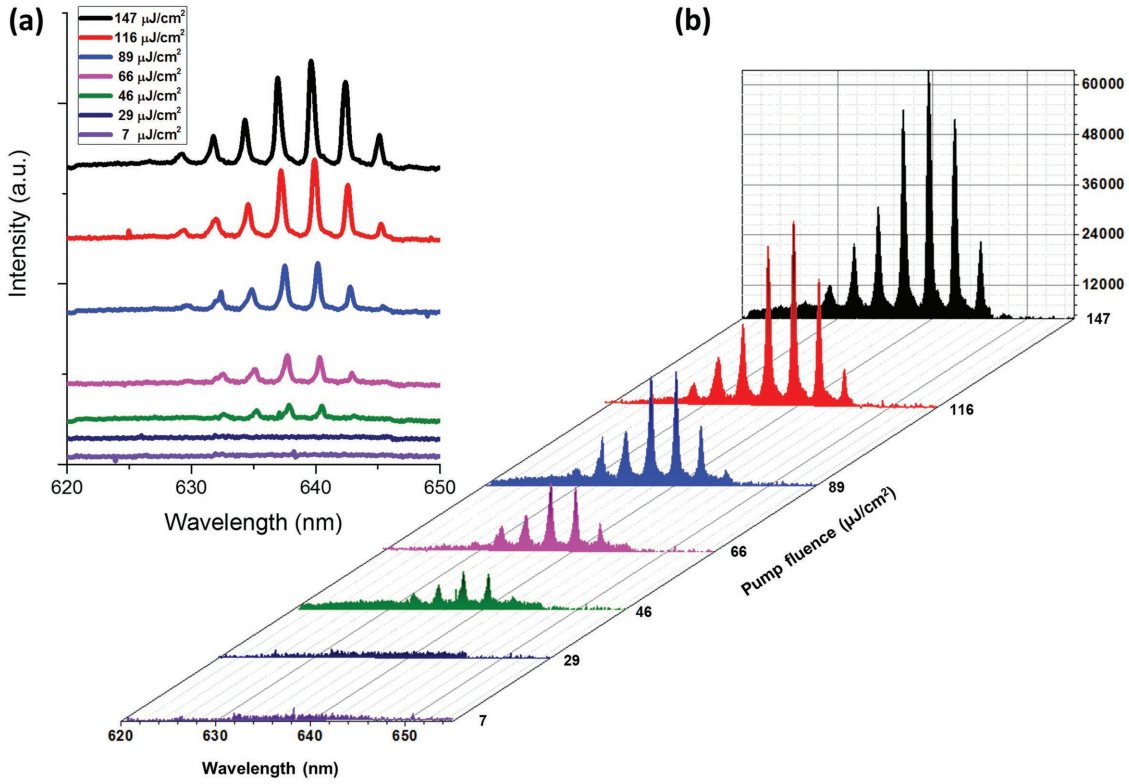

Figure 5. a) 2D and b) 3D representations of lasing spectra of QD microdisk (diameter of 26.0 μm) under varying pump fluence (F_{th} is ≈29 μJ cm^{-2}). Baselines of the 2D lasing spectra are offset for clarity.

n indicates better light confinements within the microdisks of larger diameters, which is likely due to less total internal reflection and a relatively steeper incident angle experienced by the resonant wavelength within the smaller microdisks.[42]

Next, the quality factor, which can be deduced from lasing spectra of microdisks, is an important figure of merit that indicates how well energy can be stored.[42] The quality factor is estimated as the ratio $\lambda/\delta\lambda$, where λ is the peak wavelength of the cavity mode and $\delta\lambda$ is its line width.[42] We observed that the quality factors of the dominant modes are within 1400–1650 for all microdisks with different diameters (Figure 8b). These values are comparable to those reported for other types of lasing structures using colloidal and solution-processable optically active materials (perovskite, conjugated polymer, and SiN microdisks with QDs).[23,46,47] In addition, mode splitting due to scattering centers did not reduce the quality factor of microdisks significantly. Only very modest (5%–10%) decrease in quality factor was observed in microdisks with smaller sizes (Figure S6, Supporting Information). These results demonstrate the effectiveness of the outlined fabrication approach to provide superior patterning capability while maintaining the high quality factor of robust structures of different sizes. It is worth noting that conventional top-down approaches can yield epitaxially grown QD doped microdisks that exhibit quality factors exceeding 20 000; however, as mentioned, these techniques generally require complex protocol and are not scalable.[48] Further improvement on the quality factor of our structures will be important for applications that require very narrow line width, such as for ultrasensitive sensors.

Furthermore, we observed a size dependence of the quality factor, with larger disks displaying higher values. This size dependence can be due to the higher reflectivity in larger disks that leads to better light confinement (energy storage), which is consistently in agreement with the observed trend of higher n in larger disks analyzed by using Fourier transform of emission spectra.[49] Specifically, the quality factor increased by ≈20% when the disk size changed from 10.6 to 52.1 μm. Since the lasing threshold is typically inversely proportional to the quality factor, this increase yields only a small decrease of lasing threshold and could therefore explain why the lasing thresholds of microdisks of different sizes remained on the same order of magnitude (30–90 μJ cm^{-2}) (estimated lasing threshold for microdisks ranging from 52.1–10.6 μm).[50] Besides the disk size, disk thickness can also be another factor that may affect the lasing behavior. In general, mode confinement is stronger as the thickness increases, leading to higher quality factor and lower lasing threshold. On the other hand, the peak position and number of cavity modes, determined by length of disk circumference, do not change with the disk thickness. In our specific case, rim thickness is almost constant and depends on the photoresist thickness while the center thickness grows linearly with the number of depositions. Since the mode volume is heavily concentrated along the circumference, the center thickness should not affect the optical mode confinement significantly.

The size-dependent quality factor and n of our microdisks indeed indicates that the curvature of the disk boundary plays an important role in quality factor instead of the center

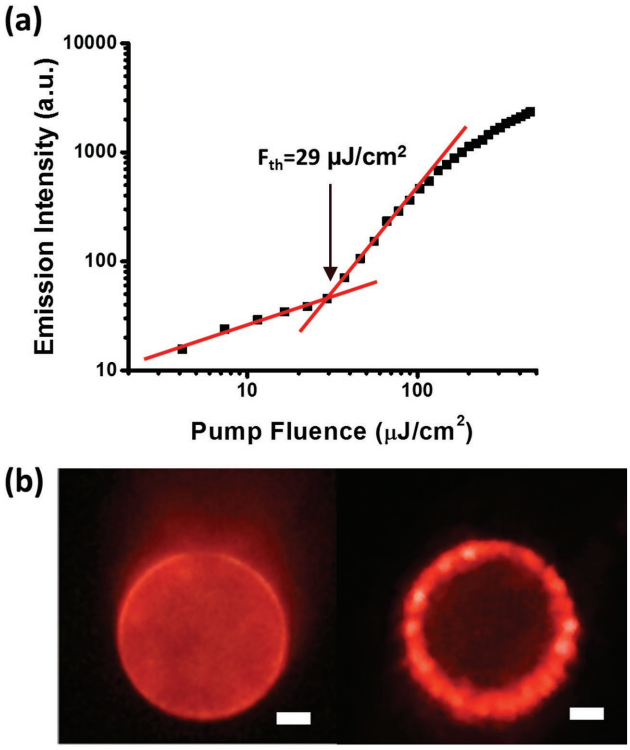

Figure 6. a) PL emission versus excitation fluence of a QD microdisk. The threshold pump fluence, F_{th} is determined from the interception of the linear and superlinear behaviors. b) PL emission images of the QD microdisk (diameter of 26.0 μm) below (left) and above (right) lasing threshold. The scale bar is 5 μm for both images.

thickness that changes from 150 nm (10.6 μm) to 100 nm (26.0, 41.6, 52.1 μm). Further optimization of the rim thickness by finite-difference time-domain (FDTD) method can be adopted in the future to improve the lasing performance. In addition, all disks have a higher quality factor at longer wavelengths (Figure S7, Supporting Information). This behavior is caused by the optical loss arising from the reabsorption of QD emission (overlap of absorption and emission bands), which is more pronounced on the lower wavelength side of the emission band (Figure S1a, Supporting Information). Overall, the quality factor of all QD microdisks fabricated here remains high, within 1000–2000, for all disks with diameters ranging from 10 to 52 μm. In addition to displaying high quality factors and low lasing thresholds, the amplified spontaneous emission intensity of our cross-linked quantum dot films is quite stable under optical pumping, as demonstrated in our recent study.[33] The combination of stable lasing output with the outlined lasing characteristics of our large-area microdisk arrays suggests that they can indeed support the development of advanced and practical photonic circuits.

3. Conclusion

We have demonstrated a viable pattern-assisted assembly process that judiciously combines the facile fabrication and precision of optical lithography for the fabrication of large-area arrays of on-chip QD microdisks with intriguing nonlinear optical characteristics. Importantly, this method mitigates limitations on the selection of active inorganic materials arising from lattice mismatch between conventional epitaxially grown semiconducting layers. Furthermore, it overcomes issues associated with predefined size, shape, and location that commonly plague the synthesis of conventional colloidal cavities grown using traditional bottom-up approaches. The combined advantages of bottom-up and top-down approaches allow for the effective production of large-scale arrays of QD microdisk lasers with controllable dimensions and locations, a feat that would be otherwise difficult to achieve using either approaches separately. Reliable tuning of the number of cavity modes and their mode spacing was successfully achieved by adjusting the diameter of the fabricated microdisks fabricated as large-area

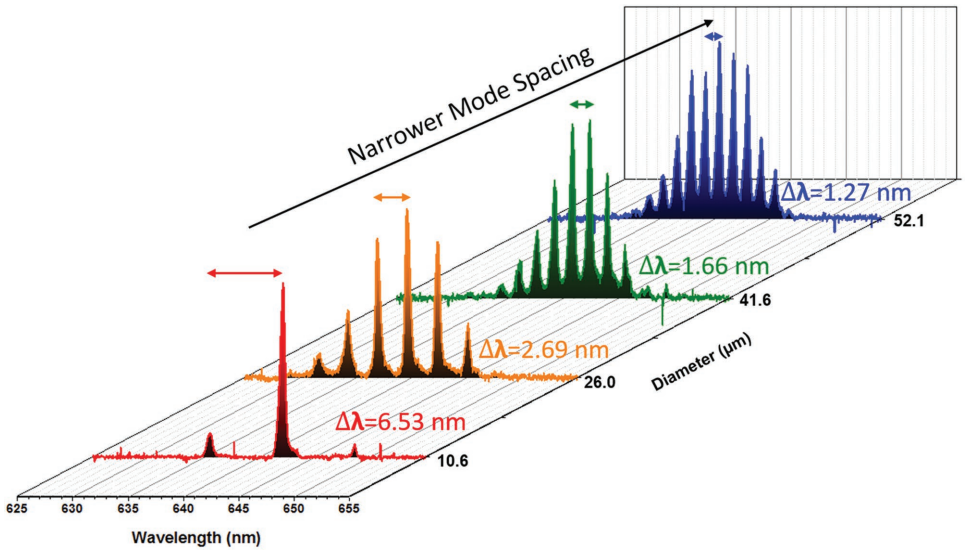

Figure 7. Lasing spectra of QD microdisks with diameter of 10.6 μm (red), 26.0 μm (orange), 41.6 μm (green), and 52.1 μm (blue). Δλ is the average mode spacing between the observed longitudinal cavity modes.

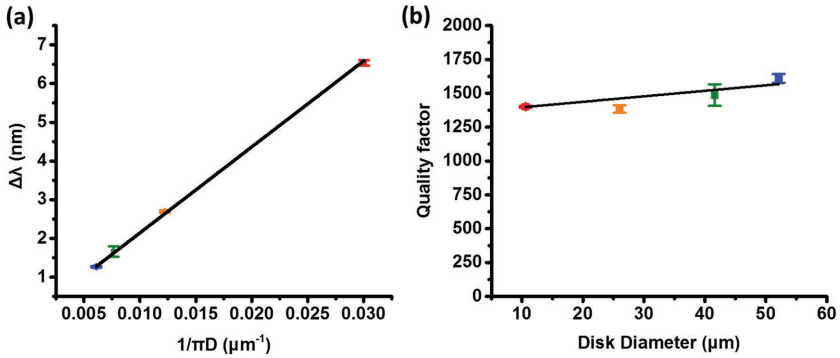

Figure 8. a) Mode spacing of cavity modes as a function of reciprocal optical path length. b) Microdisk quality factor as a function of disk diameter.

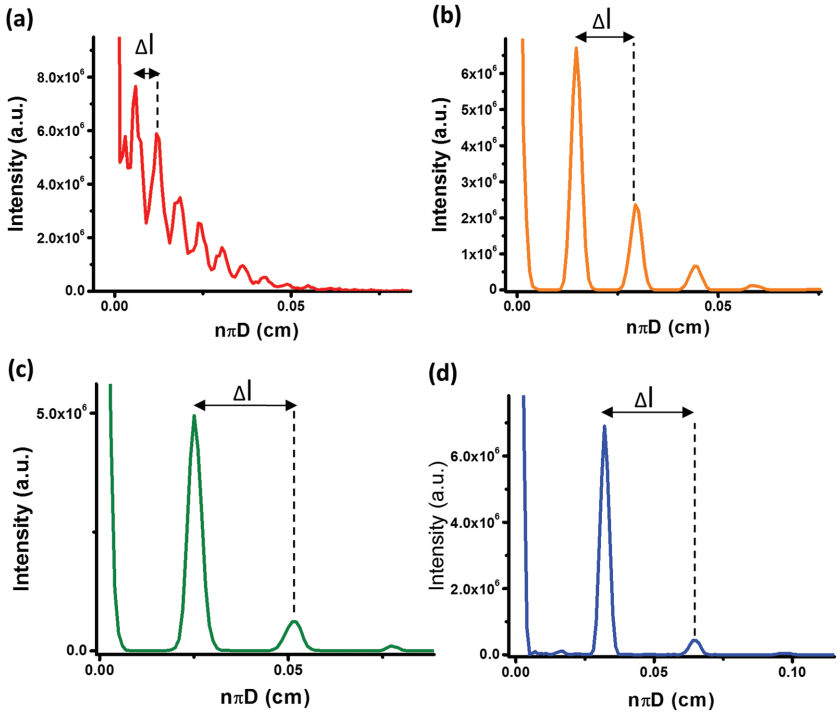

Figure 9. Fourier transform of lasing spectra from microdisks with diameters of a) 10.6 μm, b) 26.0 μm, c) 41.6 μm, and d) 52.1 μm ($\Delta l = n\pi D$).

arrays. Such tuning allowed for readily accessible multimode and near-single mode operation which can be useful in applications of optical communication, particle detection, and PT symmetry studies. Moreover, the high quality factors (1000–2000) of these robust disk arrays are comparable to reported values of microdisks made of other materials, demonstrating the capability of the outlined method to tune the size of the cavity while preserving a high quality factor.[23,46,47]

In addition, chemical cross-linking of the QDs via the bifunctional cross-linker imparts unique properties not achievable by other approaches, including mechanical robustness and chemical resistance. These properties are essential to maintain the integrity of the structures under the harsh conditions (e.g., sonication) experienced during common patterning steps (the lift-off process) and solvent exposures. We envision that the method discussed here could be potentially applied to other types of colloidal nanocrystals such as CdSe/CdS nanorods and nanoplatelets, which, unlike QDs, possess highly polarized lasing emission.[51,52] The optical anisotropy of these nanocrystals could lead to the fabrication of interesting on-chip structures with polarized lasing output that can be advantageous for many applications.[52]

Moreover, It can be further used to integrate nanocrystals with different emissions into a single structure that may lead to efficient white laser with full visible-color spectrum.[53] Furthermore, our method could be very effective at fabricating practical photonic circuits that require the integration of microdisks with specific geometry, dimension, and spectral profile on arbitrary substrates via applying a CYTOP primer layer. It is also worth mentioning that with optimized conditions, paired microdisks with submicron gaps of less than 500 nm (420 ± 51 nm) can be achieved using this method. We anticipate that this level of resolution and geometrical consistency of large-area lasing cavities with high-quality optical modes, may open up new avenues for the future development of novel stand-alone and flexible metaphotonic devices such as parity-time symmetric microcavities which might facilitate loss-less waveguiding, on-chip optical manipulation, enhanced and cleaner laser emission, omnidirectional Bragg mirrors, and other peculiar modes of light propagation.[54–58]

4. Experimental Section

Chemicals and Materials: Cadmium oxide, tri-*n*-octylphosphine (TOP, 90%), and selenium powder were obtained from Sigma-Aldrich. 1-tetradecylphosphonic acid (98%), tri-*n*-octylphosphine oxide (90%), diethylzinc (15 wt% in hexane), and hexane were obtained from Alfa Aesar. 1-octadecene (ODE, 90%), BA (98%), oleic acid (OA, 97%), and bis(trimethylsilyl) sulfide (95%) were obtained from TCI. DIAH (98%) and ethyl lactate were obtained from Sigma-Aldrich. Toluene and heptane were obtained from BDH Chemicals. CYTOP was obtained from AGC Chemicals. NR 71-3000p photoresist was purchased from Futurrex. All chemicals were used as received.

Synthesis of Compositional Gradient CdSe/Cd$_{1-x}$Zn$_x$Se$_{1-y}$S$_y$ QDs: Chemical composition gradient CdSe/Cd$_{1-x}$Zn$_x$Se$_{1-y}$S$_y$ core/graded-shell QDs were synthesized by modifying reported methods.[30,59] Briefly, 0.2 mmol of CdO, 4 mmol of Zn(acetate)$_2$, 5 mL of OA, and 15 mL of ODE were placed in a three-neck flask and degassed at 150 °C for 1 h. The reaction was heated to 300 °C under Ar. At the elevated temperature (300 °C), 1 mmol of Se and 4 mmol of S in 2 mL of TOP were rapidly injected into the reaction vessel. The reaction was allowed to proceed at 300 °C for 10 min, and then the heating mantle was removed to stop

reaction. 5 mL of hexane was added to the solution once the temperature reached 70 °C.

Optical Characterization: UV–vis extinction spectra of QD solutions (quartz cuvette) from 350 to 900 nm (1 nm intervals) were collected using a Shimadzu UV–vis–2450 spectrometer with D2 and tungsten lamps offering a wavelength range of 300–1100 nm. The QD extinction spectra were corrected against the pure solvent background and the same quartz cuvette. Photoluminescence (PL) spectra of QD solutions were collected using a Shimadzu RF-5301PC spectrofluorophotometer with the excitation wavelength of 525 nm.

PL images were collected using a Dagexcel-M Digital Firewire camera. All PL imaging was performed using photoluminescence excitation from a blue bandpass filter (450–490 nm) with a dichroic mirror that reflects optical wavelengths below 495 nm, and with a longpass emission filter that passes optical wavelengths above 500 nm. The light source was a quartz halogen lamp with an aluminum reflector, providing a wavelength range of 420–850 nm and a power of 150 W of nonpolarized light.

Fabrication of QD Microdisks: The patterning process used for fabricating QD microdisks includes several stages. First, a low refractive index layer of CYTOP (n = 1.34) was deposited on the Si wafer (n = 3.44) in order to provide light confinement within the QD cavities. A short oxygen plasma etch (5 s) was performed to improve the wettability of the CYTOP surface for the deposition of the negative photoresist (NR 71-3000p). Ethyl lactate was added to the negative resist NR 71-3000p solution to dilute it to one-third of the original concentration provided by the company. The diluted resist was spun cast on the silicon substrate (3000 rpm for 1 min). The cast film was subsequently soft baked at 165 °C for 5 min and exposed to 365 nm with a dosage of 123 mW. The exposed film was then postbaked at 100 °C for 5 min and developed by soaking in RD6 developer for 5 s. After the development, the film was rinsed with water and dried by blowing with air. The QD microdisks were fabricated by spin casting butylamine-capped QD solution (in heptane) of ≈3–6 mg mL^{-1} at 1000 rpm for 1 min onto the polymer pattern. The cast layer was subsequently immersed in 0.1 M diaminoheptane solution in methanol for 1 min and rinsed with methanol two times while spinning at 3000 rpm for 1 min. The above process was repeated multiple times to achieve the desired thickness. The polymer pattern was subsequently removed by soaking in acetone while sonicating for 3–10 s.

Confocal Micro-PL Configuration (Figure S8, Supporting Information): A Passat LTD. Compiler diode-pumped solid-state laser delivering 7 ps pulses at 532 nm with 100 Hz repetition rate was used to pump the samples. A pair of polarizers was used to control the pump fluence, I_p, while an iris was used to control the beam spot size. The pump was directed through a 40× (numerical aperture (NA) = 0.65) microscope objective using a dichroic mirror and focused on the sample. The emission was collected through the same objective, transmitted through the dichroic mirror, and focused onto a 0.5 mm diameter optical fiber coupled to a 1/2 m spectrometer and charge-coupled device (CCD) array (resolution = 0.29 nm) or collimated and projected onto a camera lens for fluorescence imaging. An additional long pass filter was used to further attenuate the reflected pump beam.

Atomic Force Microscopy: AFM images were collected using a Dimension Icon AFM microscope (Bruker) in tapping mode according to the usual procedure.[60] MikroMasch tips were used that had a spring constant of ≈7 N m^{-1}. Scan sizes of 60 µm × 60 µm with a scan rate within 0.3–0.8 Hz.

Transmission Electron Microscopy (TEM): The size of CdSe/$Cd_{1-x}Zn_xSe_{1-y}S_y$ QDs was studied using a high-resolution transmission electron microscope (Tecnai F30). An accelerating voltage of 300 keV was used. TEM samples were prepared by diluting the original QD solution of ≈6 mg mL^{-1} 30 times. 5–10 µL of the diluted solution was then drop-cast on the TEM grid and allowed to dry completely.

Scanning Electron Microscopy: SEM characterization was performed on a Hitachi S-3400N SEM with a back scattering electron detector with an accelerating voltage in the range of 5–10 kV.

Supporting Information

Supporting Information is available from the Wiley Online Library or from the author.

Acknowledgements

Financial support is acknowledged from the Air Force Office of Scientific Research FA9550-14-1-0037 (Synthetic Photonics Multidisciplinary University Research Initiative), FA9550-16-1-0187, FA9550-14-1-0269, and the UES-AFRL support S-977-022-001. M.J.S. would like to acknowledge the Science, Mathematics and Research for Transformation (SMART) scholarship funded by the OSD-T&E (Office of Secretary Defense-Test and Evaluation), Defense-Wide/PE0601120D8Z National Defense Education Program (NDEP)/BA-1, Basic Research, SMART Program office Grant No. N00244-09-1-0081.

Received: January 5, 2017
Revised: February 10, 2017
Published online:

[1] G. Agrawal, N. Dutta, *Semiconductor Lasers*, Springer, New York **1993**, p. 74.
[2] Q. J. Wang, C. Yan, N. Yu, J. Unterhinninghofen, J. Wiersig, C. Pflügl, L. Diehl, T. Edamura, M. Yamanishi, H. Kan, F. Capasso, *Proc. Natl. Acad. Sci. USA* **2010**, *107*, 22407.
[3] S. W. Eaton, A. Fu, A. B. Wong, C.-Z. Ning, P. Yang, *Nat. Rev. Mater.* **2016**, *1*, 16028.
[4] Z. Xu, Q. Liao, X. Wang, H. Fu, *Adv. Opt. Mater.* **2014**, *2*, 1160.
[5] B. R. Sutherland, E. H. Sargent, *Nat. Photonics* **2016**, *10*, 295.
[6] H. Hodaei, M.-A. Miri, M. Heinrich, D. N. Christodoulides, M. Khajavikhan, *Science* **2014**, *346*, 975.
[7] J. Zhu, S. K. Ozdemir, Y.-F. Xiao, L. Li, L. He, D.-R. Chen, L. Yang, *Nat. Photonics* **2010**, *4*, 46.
[8] R. A. Minamisawa, M. J. Süess, R. Spolenak, J. Faist, C. David, J. Gobrecht, K. K. Bourdelle, H. Sigg, *Nat. Commun.* **2012**, *3*, 1096.
[9] A. C. Scofield, S.-H. Kim, J. N. Shapiro, A. Lin, B. Liang, A. Scherer, D. L. Huffaker, *Nano Lett.* **2011**, *11*, 5387.
[10] K. H. Li, H. W. Choi, *J. Appl. Phys.* **2011**, *109*, 023107.
[11] H. Zhu, Y. Fu, F. Meng, X. Wu, Z. Gong, Q. Ding, M. V. Gustafsson, M. T. Trinh, S. Jin, X. Y. Zhu, *Nat. Mater.* **2015**, *14*, 636.
[12] S. W. Eaton, M. Lai, N. A. Gibson, A. B. Wong, L. Dou, J. Ma, L.-W. Wang, S. R. Leone, P. Yang, *Proc. Natl. Acad. Sci. USA* **2016**, *113*, 1993.
[13] Y. Wang, X. Li, J. Song, L. Xiao, H. Zeng, H. Sun, *Adv. Mater.* **2015**, *27*, 7101.
[14] C. Dang, J. Lee, C. Breen, J. S. Steckel, S. Coe-Sullivan, A. Nurmikko, *Nat. Nanotechnol.* **2012**, *7*, 335.
[15] S. T. Malak, J. Jung, Y. J. Yoon, M. J. Smith, C. H. Lin, Z. Lin, V. V. Tsukruk, *Adv. Opt. Mater.* **2016**, *4*, 608.
[16] S. T. Malak, M. J. Smith, Y. J. Yoon, C. H. Lin, J. Jung, Z. Lin, V. V. Tsukruk, *Adv. Opt. Mater.* **2016**, *5*, 1600509.
[17] S. T. Malak, E. Lafalce, J. Jung, C. H. Lin, M. J. Smith, Y. J. Yoon, Z. Lin, Z. V. Vardeny, V. V. Tsukruk, *J. Mater. Chem. C* **2016**, *4*, 10069.
[18] M. M. Adachi, F. Fan, D. P. Sellan, S. Hoogland, O. Voznyy, A. J. Houtepen, K. D. Parrish, P. Kanjanaboos, J. A. Malen, E. H. Sargent, *Nat. Commun.* **2015**, *6*, 8694.
[19] A. V. Malko, A. A. Mikhailovsky, M. A. Petruska, J. A. Hollingsworth, H. Htoon, M. G. Bawendi, V. I. Klimov, *Appl. Phys. Lett.* **2002**, *81*, 1303.
[20] M. A. Petruska, A. V. Malko, P. M. Voyles, V. I. Klimov, *Adv. Mater.* **2003**, *15*, 610.

[21] C. Grivas, C. Li, P. Andreakou, P. Wang, M. Ding, G. Brambilla, L. Manna, P. Lagoudakis, *Nat. Commun.* **2013**, *4*, 2376.
[22] Y. Chan, J. S. Steckel, P. T. Snee, J. M. Caruge, J. M. Hodgkiss, D. G. Nocera, M. G. Bawendi, *Appl. Phys. Lett.* **2005**, *86*, 073102.
[23] W. Xie, T. Stöferle, G. Rainò, T. Aubert, Y. Zhu, R. F. Mahrt, E. Brainis, Z. Hens, D. Van Thourhout, *OSA Tech. Dig.* **2016**, DOI: 10.1364/CLEO_AT.2016.JTh4B.6.
[24] B. De Geyter, K. Komorowska, E. Brainis, P. Emplit, P. Geiregat, A. Hassinen, Z. Hens, D. Van Thourhout, *Appl. Phys. Lett.* **2012**, *101*, 161101.
[25] J. M. Luther, M. Law, Q. Song, C. L. Perkins, M. C. Beard, A. J. Nozik, *ACS Nano* **2008**, *2*, 271.
[26] C. Jiang, V. V. Tsukruk, *Adv. Mater.* **2006**, *18*, 829.
[27] G. I. Koleilat, L. Levina, H. Shukla, S. H. Myrskog, S. Hinds, A. G. Pattantyus-Abraham, E. H. Sargent, *ACS Nano* **2008**, *2*, 833.
[28] L. Feng, Z. J. Wong, R.-M. Ma, Y. Wang, X. Zhang, *Science* **2014**, *346*, 972.
[29] B. Peng, S. K. Ozdemir, F. Lei, F. Monifi, M. Gianfreda, G. L. Long, S. Fan, F. Nori, C. M. Bender, L. Yang, *Nat. Phys.* **2014**, *10*, 394.
[30] W. K. Bae, K. Char, H. Hur, S. Lee, *Chem. Mater.* **2008**, *20*, 531.
[31] Y. Wang, S. Yang, H. Yang, H. Sun, *Adv. Opt. Mater.* **2015**, *3*, 652.
[32] J. Jung, C. H. Lin, Y. J. Yoon, S. T. Malak, Y. Zhai, E. L. Thomas, V. Vardeny, V. V. Tsukruk, Z. Lin, *Angew. Chem.* **2016**, *128*, 5155.
[33] C. H. Lin, E. Lafalce, J. Jung, M. J. Smith, S. T. Malak, S. Aryal, Y. J. Yoon, Y. Zhai, Z. Lin, Z. V. Vardeny, V. V. Tsukruk, *ACS Photonics* **2016**, *3*, 647.
[34] C. A. Mack, *Fundamental Principles of Optical Lithography: the Science of Microfabrication*, John Wiley & Sons Ltd., Chichester, UK **2012**.
[35] G. Decher, J. B. Schlenoff, *Multilayer Thin Films: Sequential Assembly of Nanocomposite Materials*, Wiley-VCH, Weinheim, Germany **2012**.
[36] X. Lan, O. Voznyy, A. Kiani, F. P. García de Arquer, A. S. Abbas, G.-H. Kim, M. Liu, Z. Yang, G. Walters, J. Xu, M. Yuan, Z. Ning, F. Fan, P. Kanjanaboos, I. Kramer, D. Zhitomirsky, P. Lee, A. Perelgut, S. Hoogland, E. H. Sargent, *Adv. Mater.* **2016**, *28*, 299.
[37] Y. Kim, E. Yassitepe, O. Voznyy, R. Comin, G. Walters, X. Gong, P. Kanjanaboos, A. F. Nogueira, E. H. Sargent, *ACS Appl. Mater. Interfaces* **2015**, *7*, 25007.
[38] Y. Zhao, K. Zhu, *J. Phys. Chem. Lett.* **2013**, *4*, 2880.
[39] R. Suntivich, I. Drachuk, R. Calabrese, D. L. Kaplan, V. V. Tsukruk, *Biomacromolecules* **2014**, *15*, 1428.
[40] P. J. Yunker, T. Still, M. A. Lohr, A. G. Yodh, *Nature* **2011**, *476*, 308.
[41] Y. Wang, K. E. Fong, S. Yang, Van D. Ta, Y. Gao, Z. Wang, V. Nalla, H. V. Demir, H. Sun, *Laser Photonics Rev.* **2015**, *9*, 507.
[42] S. Yang, Y. Wang, H. Sun, *Adv. Opt. Mater.* **2015**, *3*, 1136.
[43] Z. Li, Z. Zhang, T. Emery, A. Scherer, D. Psaltis, *Opt. Express* **2006**, *14*, 696.
[44] L. He, S. K. Ozdemir, J. Zhu, W. Kim, L. Yang, *Nat. Nanotechnol.* **2011**, *6*, 428.
[45] R. C. Polson, G. Levina, Z. V. Vardeny, *Appl. Phys. Lett.* **2000**, *76*, 3858.
[46] R. C. Polson, Z. V. Vardeny, D. A. Chinn, *Appl. Phys. Lett.* **2002**, *81*, 1561.
[47] H. Zhang, Q. Liao, X. Wang, J. Yao, H. Fu, *Adv. Opt. Mater.* **2016**, *4*, 1718.
[48] Q. Song, W. Fang, B. Liu, S.-T. Ho, G. S. Solomon, H. Cao, *Phys. Rev. A* **2009**, *80*, 041807.
[49] Y. Zhang, M. Lončar, *Opt. Express* **2008**, *16*, 17400.
[50] D. J. Gargas, M. C. Moore, A. Ni, S.-W. Chang, Z. Zhang, S.-L. Chuang, P. Yang, *ACS Nano* **2010**, *4*, 3270.
[51] Y. Gao, V. D. Ta, X. Zhao, Y. Wang, R. Chen, E. Mutlugun, K. E. Fong, S. T. Tan, C. Dang, X. W. Sun, H. Sun, H. V. Demir, *Nanoscale* **2015**, *7*, 6481.
[52] M. Li, M. Zhi, H. Zhu, W.-Y. Wu, Q.-H. Xu, M. H. Jhon, Y. Chan, *Nat. Commun.* **2015**, *6*, 8513.
[53] F. Fan, S. Turkdogan, Z. Liu, D. Shelhammer, C. Z. Ning, *Nat. Nanotechnol.* **2015**, *10*, 796.
[54] K. G. Makris, R. El-Ganainy, D. N. Christodoulides, Z. H. Musslimani, *Phys. Rev. Lett.* **2008**, *100*, 103904.
[55] Z. Lin, H. Ramezani, T. Eichelkraut, T. Kottos, H. Cao, D. N. Christodoulides, *Phys. Rev. Lett.* **2011**, *106*, 213901.
[56] H. Ramezani, T. Kottos, R. El-Ganainy, D. N. Christodoulides, *Phys. Rev. A* **2010**, *82*, 043803.
[57] A. Regensburger, C. Bersch, M. A. Miri, G. Onishchukov, D. N. Christodoulides, U. Peschel, *Nature* **2012**, *488*, 167.
[58] M. A. Noginov, G. Zhu, A. M. Belgrave, R. Bakker, V. M. Shalaev, E. E. Narimanov, S. Stout, E. Herz, T. Suteewong, U. Wiesner, *Nature* **2009**, *460*, 1110.
[59] W. K. Bae, M. K. Nam, K. Char, S. Lee, *Chem. Mater.* **2008**, *20*, 5307.
[60] M. E. McConney, S. Singamaneni, V. V. Tsukruk, *Polym. Rev.* **2010**, *50*, 235.